



Effect of lattice stacking orientation and local thickness variation on the mechanical behavior of few layer graphene oxide



Teng Cui ^{a,1}, Sankha Mukherjee ^{b,1}, Changhong Cao ^a, Parambath M. Sudeep ^a, Jason Tam ^b, Pulickel M. Ajayan ^c, Chandra Veer Singh ^{b,***}, Yu Sun ^{a,**}, Tobin Filleter ^{a,*}

^a Department of Mechanical and Industrial Engineering, University of Toronto, Toronto, ON, M5S 3G8, Canada

^b Department of Materials Science and Engineering, University of Toronto, Toronto, ON, M5S 3E4, Canada

^c Department of Materials Science and NanoEngineering, Rice University, Houston, TX, 77005, United States

ARTICLE INFO

Article history:

Received 23 March 2018

Received in revised form

20 April 2018

Accepted 24 April 2018

Available online 27 April 2018

ABSTRACT

Investigation of few layer 2D materials is fundamentally important to bridge the gap between monolayer and bulk properties, and practically meaningful for applications as reinforcement nanofillers and layered electronic devices. Few layer introduces differences from intrinsic properties of monolayers due to the complexity of structural heterogeneities, such as lattice stacking orientation and local thickness variation. In this work, few layer graphene oxide (GO) with different structural heterogeneities were studied using atomic force microscopy-based deflection measurements and transmission electron microscopy (TEM). Direct TEM evidence of fracture surfaces and molecular dynamics (MD) simulations revealed decoupled and dissimilar layer crack patterns for misaligned bilayer. In contrast, aligned bilayer GO generally fractured with a larger portion of common cracks shared by both layers, indicating stronger interlayer interaction. MD results also revealed insignificant effect of lattice alignment on the strength and toughness of GO bilayers. Scaling up even to ~5 layers and above revealed significant local thickness heterogeneity and consequently a ~60% reduction of the normalized fracture force and toughness. MD simulations on partially intercalated few layer GO revealed anisotropic and heterogeneous stress distributions, as well as stress concentration near the inner edges, which may account for the significant reduction of strength and toughness.

© 2018 Elsevier Ltd. All rights reserved.

1. Introduction

Single atomic layer graphene exhibits unprecedented strength and stiffness [1,2], which has motivated the investigation and application of a variety of 2D materials and their variations with unique mechanical properties [3–6]. Graphene oxide (GO), a functionalized form of graphene, is composed of oxygen-containing functional moieties on its carbon basal plane which include epoxide, hydroxyl, and carboxylic acid groups [7]. Control of these functional groups endows GO tunable mechanical properties with varying Young's modulus and strength [3,8–10]. However, one

major bottleneck in the large-scale application of GO lies in the difficulties of preparing monolayer GO with large lateral sizes [11]. Therefore, multilayer GO with larger lateral dimension are of practical importance, especially in macroscopic applications, including as reinforcement nanofillers for light-weight nanocomposites [12,13], as solid lubricants [14], and as supporting platform for supercapacitors [15,16]. Nevertheless, there is a clear size-scale effect in the mechanical properties of GO. Take GO strength as an example, the strength of monolayer GO (thickness ~0.7–1.2 nm) is 24.7 GPa [8], which is approximately twice that of GO nanosheets (thickness: ~10–100 nm) [17]. GO paper with thickness of more than 1 μm has a strength of only ~100 MPa [18,19], which is two orders of magnitude lower than its monolayer counterpart. Therefore, one challenge in translating the extraordinary mechanical properties of GO to real applications is to understand and bridge the gap in our understanding of monolayer and multilayer properties.

As the first and most fundamental step to scale up to multilayer,

* Corresponding author.

** Corresponding author.

*** Corresponding author.

E-mail addresses: chandraseer.singh@utoronto.ca (C.V. Singh), sun@mie.utoronto.ca (Y. Sun), filleter@mie.utoronto.ca (T. Filleter).

¹ These authors contributed equally.

the interaction between bilayer must be understood. It has been widely demonstrated that graphitic bilayers can be stacked at different lattice orientations [3,20,21], which has been shown to influence the electronic characteristics [22]. However, the investigation of such a stacking effect on mechanical properties is limited and has primarily focused on friction, such as studies on graphite which have revealed superlubricity when stacking at incommensurate angles other than 0° and 60° [23]. Moreover, existing studies have focused on graphene. There is no report of lattice stacking orientation effect on the fracture behaviors of GO bilayers. Compared with graphene, GO can be more complex due to the presence of functional groups with different chemical nature and heterogeneous distribution [7,24]. In addition to lattice stacking orientation, additional structural heterogeneities, such as wrinkles and folds also exist, primarily due to uncontrolled capillary flow and de-wetting during solvent evaporation process [25,26]. Consequently, when scaling up the thickness from monolayers to multilayers, GO with different lateral sizes can possess aggregates and partial intercalation of discontinuous layers [25]. Such detailed investigation of the structural heterogeneity effect on the mechanical properties of few layer GO is critical yet still missing.

Herein, we report the effect of two important structural heterogeneities, lattice stacking orientation and local layer thickness variation, on the mechanical behavior of few layer GO, and further elucidate the size-scale effect for ultrathin GO membranes with thickness varying from single to ~ 15 layers. Bilayer GO with different lattice stacking angles were prepared and characterized using atomic force microscopy (AFM)-based deflection measurements and transmission electron microscopy (TEM). Post-mortem fracture surface analysis and extensive molecular dynamics (MD) simulations revealed distinct cracking behavior for aligned and misaligned GO. Furthermore, we have demonstrated $\sim 60\%$ deterioration in the normalized strength and toughness of GO caused by local thickness variation when scaling up even to five atomic layers. Potential mechanisms for such degradation in properties were investigated using MD simulations.

2. Experimental and computational methods

2.1. GO synthesis and membrane preparation

GO was prepared by using an improved Hummers method reported elsewhere [27]. For the synthesis of GO, 1 g of graphite powder (SP1 Graphite, Bay Carbon) was dispersed in a 9:1 mixture of $\text{H}_2\text{SO}_4:\text{H}_3\text{PO}_4$ (Sigma Aldrich) and stirred at 50°C for 2 h. 6 g of KMnO_4 (Sigma Aldrich) was then added to the mixture in parts. The addition of KMnO_4 resulted in an exothermic reaction with an increase in temperature to 90°C . Upon addition of KMnO_4 , the color of the solution changed from black to dark brown, after which the mixture was subjected to continuous stirring overnight. The mixture was then poured over ice, and 6–8 mL H_2O_2 added slowly which resulted in effervescence and evolution of yellowish-brown color. The precipitate was then transferred out; it was washed two times with 100 ml of water, 100 ml of 30 wt% HCl, and 100 mL ethanol. In order to prepare suspended GO membranes, the synthesized GO powders were then dispersed in deionized water in a concentration of 1 mg GO:20 mL water. Then the solution was gently agitated for two weeks using a magnetic stirrer for exfoliation. Such an exfoliation method yielded larger GO flakes as compared to ultra-sonication, enabling the samples to cover multiple holes with a single flake. After that, the upper aqueous solution was mixed with methanol in a ratio of 1:3, followed by two steps of centrifugation [28]. First, the solution mixture was centrifuged at 8000 rpm for 20 min to remove supernatant containing small GO flakes. Then, the precipitate was collected and re-

dispersed in a solution of 1:3 mixture of $\text{H}_2\text{O}:\text{methanol}$, which was further centrifuged at 2500 rpm for 10 min. The upper solution was then drop-casted on perforated TEM grids to form suspended membranes. The prepared GO membranes were stored at controlled $20 \pm 5\%$ relative humidity and further tested under the same ambient environment.

2.2. GO sample characterization

The oxidation degree of the GO sample was characterized by X-ray photoelectron spectroscopy (XPS) using Thermo Scientific K-Alpha XPS system (ThermoFisher Scientific, E. Grinstead, UK) equipped with combined Ar^+/e^- flood gun. Monochromatic aluminum K_{α} X-ray was applied over a spot size of $400 \mu\text{m}$. The XPS data was processed using CasaXPS software. The prepared GO membranes were examined and characterized by both SEM and TEM. SEM was conducted using Hitachi S-4800 instrument with an acceleration voltage of 1 kV and an electron beam current of $2 \mu\text{A}$. The TEM images and selected area electron diffraction (SAED) patterns were obtained under 100 kV using Hitachi HF-3300 TEM. AFM topographical imaging was conducted before and after deflection test in AC mode by Asylum MFP-3D AFM using monolithic diamond probes (NadiaProbes, Catalogue #: ND-DYIRS-5, $k = 35 \text{ N/m}$, $f = 310 \text{ kHz}$). A scan rate of 1 Hz and 256×256 Points & Lines were applied for all the AFM imaging. Mechanical properties of the GO membranes were characterized by AFM deflection testing using the same AFM and diamond probes as for topographical imaging. In order to capture the cracking behavior rather than puncturing a hole of the membrane, low aspect ratio blunt tips are preferred than high aspect ratio sharp tip. The diamond probes used in this work are of four-sided pyramid shape with tip radius of $\sim 65 \text{ nm}$ (see Supporting Information Figure S6). The stiffness of the cantilever was calibrated using Sader method [29]. The membranes were deflected 600 nm in total under displacement control at a constant rate of 100 nm/s.

2.3. Molecular dynamics simulations

MD simulations were performed using the LAMMPS package [30], with inter-atomic interactions described by the ReaxFF potential [31]. The ReaxFF potential has been used in a host of previous works on the mechanical properties of GO systems of various compositions. For preparing the MD model, the atoms belonging to the hydroxyl and the epoxide functional groups were attached to the carbon basal planes. The GO nanosheets were 70% functionalized in the basal plane with an epoxide-to-hydroxyl ratio of approximately 4:1. The locations of these groups were selected randomly, and equal weightages were assigned to location on both sides of the carbon basal planes. For the bilayer GO samples, the simulation cells were 16.3 nm and 17.8 nm along the in-plane directions with a thickness of 1.25 nm. Periodic boundary conditions were applied along the in-plane directions. In the thickness direction, a vacuum of 20 \AA was used on both sides. The nearest neighbor and hydrogen bond cut-off radii were set to 5 and 7.5 \AA , respectively. Starting from 1 K, the temperature of the GO samples were gradually raised to 300 K over a period of 25 ps and then thermally equilibrated at 300 K in a NPT ensemble. The thermal equilibration is essential to minimize the system pressure and allow for cell relaxation. Here, N stands for number of atoms, P represents pressure, and T is temperature. Inside the ensemble, N, P and T are maintained constant. The simulation time step was 0.25 fs and the damping parameter for the Nose-Hoover thermostat was 25 fs. Equibiaxial strain-controlled tensile loading was imposed by dilating the simulation box along both in-plane directions and simultaneously performing an equivalent affine transformation to

the constituent atomic positions. Stress was calculated using the Virial theorem, and a strain rate of $10^9/s$ was used for all the simulations. The Open Visualization Tool (Ovito) was used to visualize atomic structures.

3. Results and discussion

3.1. Effect of lattice stacking orientation

The GO samples studied here were synthesized following the improved Hummers method [27], which has been shown to yield highly oxidized GO with epoxide-rich functional groups [9]. Fig. 1a shows the XPS spectrum of GO with ~70% oxidation, which agrees well with literature [9,27]. GO membranes were prepared by a solution-based drop-casting method [8,28] onto silicon nitride TEM grids containing arrays of circular holes. Fig. 1b shows the SEM image of one GO flake on a TEM grid. TEM bright field imaging (Fig. 1c) revealed no obvious contaminants or major defects of the GO membranes. Ultrathin GO membranes as thin as single layer were obtained. The SAED pattern in Fig. 1d revealed one set of six diffraction spots. Moreover, the inner diffraction spots also show higher intensity than outer diffraction spots, which is confirmed to be monolayer [32,33]. To study the role of stacking orientation, a number of bilayer GO membranes were prepared and the SAED was utilized to count the number of layers and measure stacking angles, following a procedure used in previous literature [3,21,34]. The bilayer GO was determined by two sets of diffraction spots, together with a stronger inner diffraction intensity. It is noted that we do not have a direct control of the stacking angle in the sample preparation process. However, well-aligned ($<5^\circ$) and largely misaligned bilayer GO ($>20^\circ$) were commonly obtained, in accordance with previous studies on graphene which revealed that 0° and 30° are preferred stacking angles [20]. Schematics of bilayer GO stacking at 0° and 30° are shown in Fig. 1e and f (only the carbon skeleton is shown for clarity). Fig. 1g and h are examples of aligned and misaligned bilayer GO stacking at 3.3° and 29.6° , respectively. Due to the existence and interaction of functional groups, out-of-plane waviness and in-plane distortion can be present [24], making exact 0° stacking unlikely across an area, particularly for the highly oxidized GO studied in this work. Therefore, we arguably classify stacking angles of less than 5° as the aligned case, greater than 20°

as the largely misaligned case. Moreover, for each sample, SAED was performed in three different regions to ensure overall homogeneity in terms of both the number of layers and stacking angle for bilayer GO.

Bilayer GO membranes with different stacking angles were mechanically loaded till complete fracture by AFM deflection testing. It was deemed as a complete fracture when the force dropped to or below half of the maximum force. It has been noticed that the suspended GO membranes have initial sag depth, which invalidates the commonly adopted model for, e.g., graphene, mechanical properties calculation [1]. A combined experimental and finite element analysis of sag effect on the deflection measurement and fracture morphology is discussed in detail in Section 1 of Supporting Information, and the results revealed visible cracking patterns for the deeply sagged membranes after fracture. Therefore, we did not use the model and instead chose to report only forces and energy directly, and emphasis was focused on the fracture behavior of bilayer GO with different stacking angle. All the following discussions consider membranes having similar initial sag depths. Representative AFM deflection curves of bilayer GO with 3.2° and 23.2° stacking angles are shown in Fig. 2a (see Supporting Information Figure S1 for all five bilayer samples studied). All the membranes have an initial sag depth in a close range of $0.16\text{--}0.17\ \mu\text{m}$ (Fig. 2b,d) across a $2.5\ \mu\text{m}$ diameter span. AFM topographical imaging of fractured surfaces (Fig. 2c,e) revealed morphology of cracking lines rather than holes for both stacking angles due to the membrane sag, which enables a detailed TEM analyses of the fracture pattern.

Post-mortem TEM imaging revealed that the crack width for the aligned bilayer GO (Fig. 3a) was $\sim 10\ \text{nm}$, which is narrower than the crack width in the misaligned bilayer (Fig. 3b). Moreover, Fig. 3b revealed that in the misaligned case cracks do not only occur at the same position for both layers, but can also propagate within each individual layers independently. In Fig. 3b and c, regions of bilayer, monolayer, and hole could be clearly identified based on the TEM image contrast. Interestingly, bilayer region surrounded by monolayer GO was also observed in the misaligned bilayer (Fig. 3c). Possible explanation for such morphology is that cracking took place on both layers along different directions but with a shared non-fractured area stacking together, as was also predicted by MD simulations (Fig. 3e). In this case, the single layer region to the right

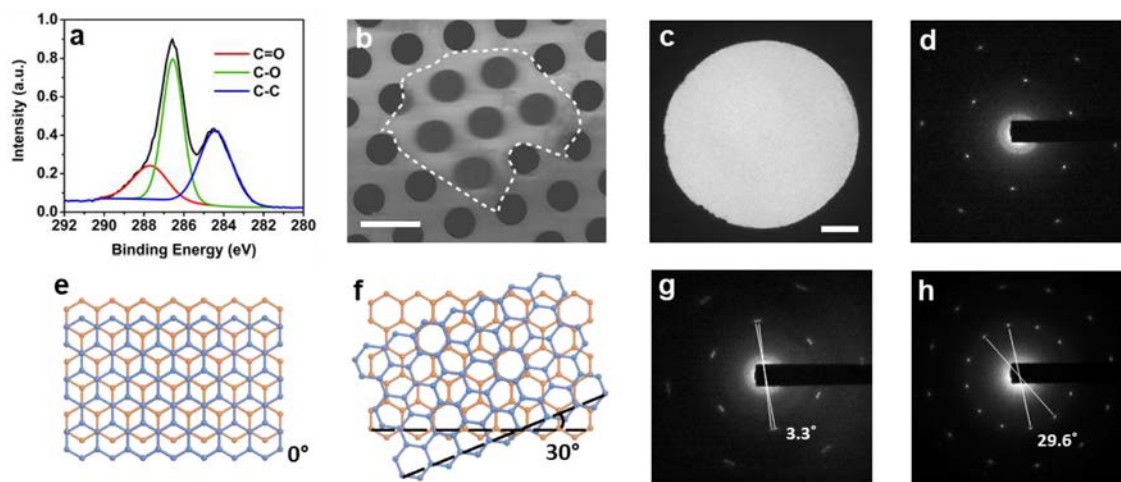


Fig. 1. Chemical and structural characterization of bilayer GO samples. (a) C1s XPS spectrum of the synthesized GO. (b) SEM image of GO membrane suspended on holey TEM grid (GO enclosed by white dashed line). Scale bar, $5\ \mu\text{m}$. (c) TEM bright field image of a suspended bilayer GO showing no obvious contamination or major defects. Scale bar, $500\ \text{nm}$. (d) SAED pattern of monolayer GO. (e,f) Schematics of bilayer GO stacking at 0° and 30° , only the carbon skeleton is shown for clarity. (g,h) SAED patterns of bilayer GO stacking at 3.3° and 29.6° . (A colour version of this figure can be viewed online.)

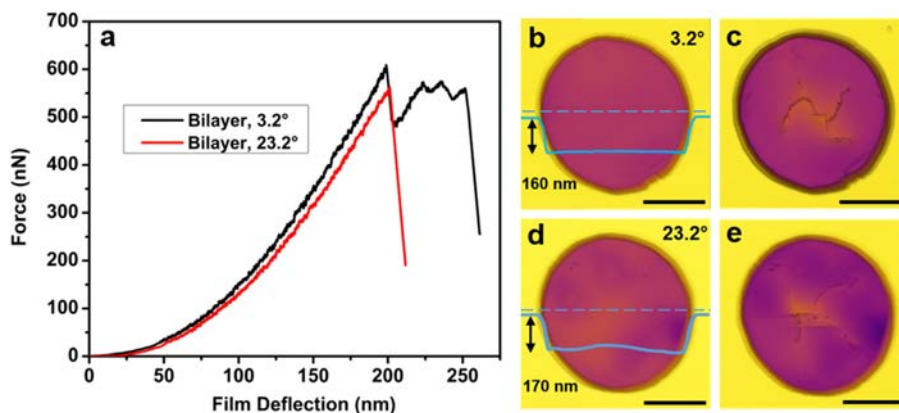


Fig. 2. AFM deflection tests of aligned and misaligned bilayer GO. (a) Force–deflection curves of bilayer GO membranes with different stacking angles. (b,c) AFM topographical images for bilayer GO of 3.2° stacking angle before and after deflection test. (d,e) AFM topographical images for bilayer GO of 23.2° stacking angle before and after deflection test. Scale bars, 1 μm . (A colour version of this figure can be viewed online.)

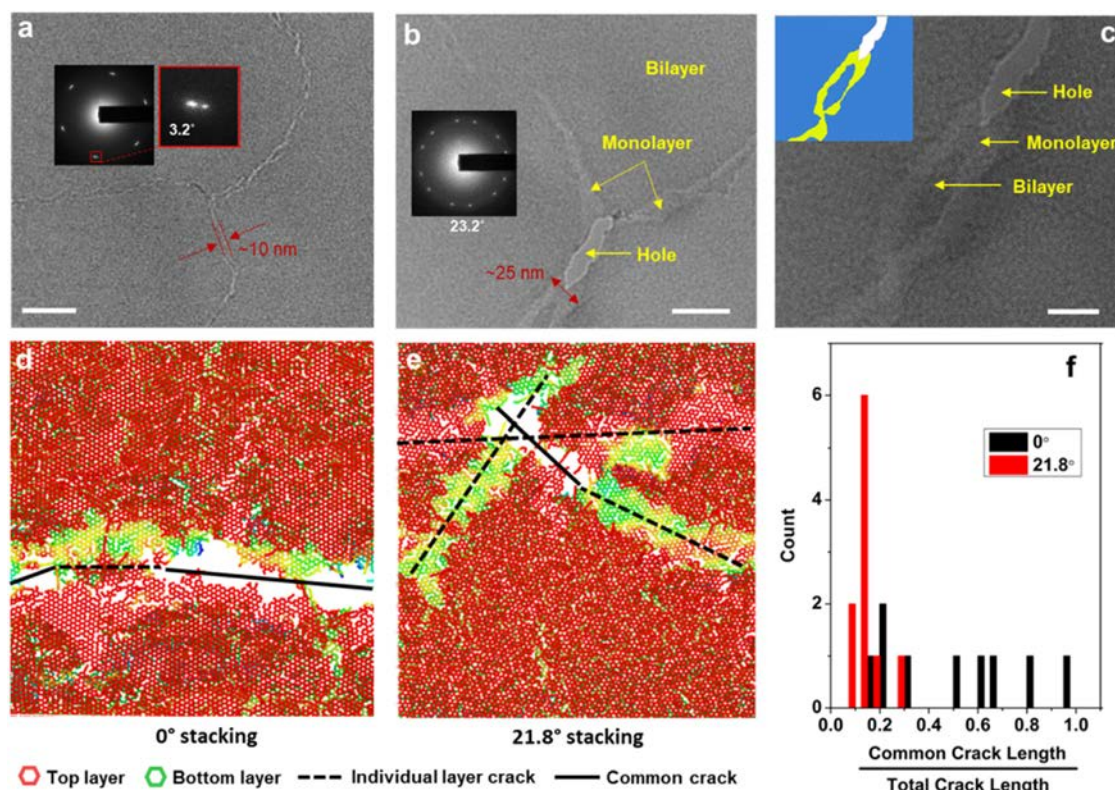


Fig. 3. Effect of lattice stacking orientation on bilayer GO fracture. (a) TEM image of fracture surface for aligned (3.2° stacking angle) bilayer GO showing narrow and similar cracking path for both layers. Insets: SAED pattern and a zoom-in view of one set of diffraction spots showing bilayer GO. Scale bar: 100 nm. (b,c) TEM fracture surfaces of misaligned (23.2° stacking angle) bilayer GO showing individual layer cracking. Insets: (b) SAED pattern of bilayer GO stacking at 23.2°. (c) False colored image highlighting regions of different layers. Scale bars: 40 nm, b; 20 nm, c. (d,e) Representative MD simulation results of bilayer GO showing higher percentage of common fracture path for 0° stacking and individual layer cracking for 21.8° stacking. Colors in (d,e) represent out-of-plane position gradient, with red is top layer and green is the bottom layer. The simulation cell size is 16.3 nm by 17.8 nm. (f) Histogram of the ratio between common crack length and total crack length for both stacking angles from MD simulations. (A colour version of this figure can be viewed online.)

and left of the central bilayer area is not the same layer. Similar behaviors, i.e., dissimilar crack propagation in individual atomic layers, shearing, and pullout, were not observed in the aligned case, which also explains why the crack is narrower for the aligned bilayer.

To further understand the underlying fracture mechanisms, MD simulations were performed for bilayer GO samples with 0° and 21.8° stacking angles to represent the aligned and a misaligned

bilayer (similar to Fig. 1e and f). Equibiaxial strain-controlled tensile loading was chosen to reflect the stress state of the membrane at the loading point in AFM deflection experiments. At the scale of the whole MD cell size (16.3 nm by 17.8 nm), the GO model can be approximately regarded as isotropic within the plane, as proved by the similar stress–strain behavior along both x and y directions with ~2% of difference in strength (see Supporting Information Table S2). Additionally, according to the stress transformation theory in

continuum mechanics, for equibiaxial strain loading, every point in the GO structure should experience similar stress magnitude along the in-plane directions, which emulates the stress state at the loading point in experiments. Previous investigations on the structure of GO demonstrated that oxygen functional groups tend to form localized island structures instead of a homogeneous distribution [35,36]. In order to capture the effect of the stochasticity associated with the dispersion of the functional groups on the fracture propagation, a set of twenty MD samples with stacking angles of 0° and 21.8° were biaxially strained to fracture. Fig. 3d and e shows representative fracture surfaces for a 0° and 21.8° stacked GO bilayer (see Supporting Information Figure S4 for additional examples), revealing overlapped and dissimilar fracture path, respectively, in good agreement with experimental observation. Distinct colors represent different out-of-plane positions of the atoms, with atoms in the top layer colored red and those in the bottom layer colored green. Further analysis was conducted by differentiating individual layer cracks with common bilayer cracks. Here, individual layer cracks refer to cases where the fracture only occurred in one of the two layers at a position and did not transfer to adjacent layer; thus the fracture pathways in constituent layers are distinctly dissimilar. Meanwhile, common bilayer cracks refer to cases where crack transferred to adjacent layer at the same position; therefore, the fracture pathways in both layers are largely similar. The ratio between common crack length and total crack length (addition of common and individual layer crack lengths) for both stacking angles is summarized in a histogram (Fig. 3f). A higher ratio means easier to transfer crack to adjacent layer, thus indicating stronger interlayer interaction. It is interesting that for the aligned bilayer GO, the fracture path was found to be mostly random for both layers instead of consistently sharing the same fracture path. Furthermore, it was also observed in an extreme case of aligned bilayer that the top and bottom layer revealed completely dissimilar fracture path (see Supporting Information Figure S4). Such scattered behavior revealed that the interlayer interaction in aligned GO bilayers is not sufficiently strong to consistently transfer cracks to adjacent layer for different cases with varying distribution of functional groups. However, the misaligned GO bilayers revealed even weaker interlayer interaction by consistently exhibiting dissimilar fracture pathways for the constituent layers for all the cases. The reason for the weak interaction for both aligned and misaligned bilayer could be due to the epoxide-rich functional groups in the GO studied here. Previous studies reported that the interlayer interaction of epoxide-rich GO is weaker as compared to hydroxyl-rich GO due to limited hydrogen bonds between layers [17]. The relatively weaker interlayer interaction for misaligned bilayer GO could also be related to the superlubricity of graphite at misaligned stacking [23].

It is important to note that some bilayer membranes, including both aligned and largely misaligned GO bilayers, experienced a stepwise fracture behavior with small force drops in the deflection curve (see Fig. 2a and Supporting Information Figure S1, S3), similar to those observed by Lin et al. [37] in stacked bilayer graphene. Such stepwise fracture was not found to be directly related to a particular stacking angle. Lin et al. [37] ascribed this stepwise behavior to sequential fracture in different graphene layers. Additionally, in their bilayer graphene case, there was only one occurrence of force drop before a catastrophic rupture. However, for the GO samples studied here, curves with no stepwise force drop, only one drop, as well as several stepwise force drops were all observed both in experiments and in simulations. For example, for the bilayer GO sample with 3.2° stacking angle shown in Fig. 2a, four force drops were observed, indicative of progressive fracture occurring in each atomic carbon layer. Such a phenomenon can be due to the elastoplastic nature of the highly oxidized epoxide-rich GO [9] where

cracks can initiate at multiple defective sites. In addition, we have also observed that the functional groups can serve as crack arresters and increase the fracture toughness, thus delaying catastrophic failure once after crack initiation [38], which is consistent with the AFM deflection results and MD simulations. MD simulations revealed a strength and toughness (the area under the stress-strain curve in a full range to failure) of 23.84 GPa and 1.71×10^{-18} J/nm³ for aligned GO bilayer, and 23.35 GPa and 1.66×10^{-18} J/nm³ for misaligned GO bilayer. It should be noted that this difference is insignificant and generally within the error bars (see Supporting Information Figure S3, Table S2). Wei et al. [39] performed indentation simulations on aligned and misaligned graphene multilayers using coarse-grained MD, and revealed higher strength for the aligned samples with three or more layers. This is also consistent with the fracture behavior observed herein which indicates that the aligned GO samples exhibit stronger interaction between layers, thus leading to a higher strength and toughness. However, both the experimental and MD results suggest that such a lattice stacking orientation effect on strength is not significant for bilayer GO stacking, and instead the most significant difference is in the post yield fracture behavior.

3.2. Effect of local thickness variation

In the above results, the lattice stacking orientation was shown to have a significant effect on the fracture pathways rather than the strength of GO. Whereas in the following, we show that the strength and toughness can be significantly influenced by the second type of heterogeneity, i.e., local thickness variation due to multiple layer stacking. With increasing number of layers, it is likely that the effect of lattice stacking orientation would be reduced due to the increased probability of many randomly oriented lattices as the thickness increases. The toughness is defined by the area under the full range of force-deflection curve to failure, which is also the energy-to-failure. It is documented that wrinkles can significantly affect the elastic modulus of GO papers, however do not significantly affect monolayer GO [40]. Previous investigations [17] also revealed a size-scale dependency of the mechanical properties on GO thickness and suggested a transition from intraplanar to interplanar fracture mechanism when scaling from GO monolayer to its bulk paper form. However, a more detailed and elusive question is how many layers are needed to maintain the intrinsic monolayer strength of GO. A recent study [41] on atomically thin boron nitride revealed almost no strength loss with increasing thickness of up to 9 layers, whereas, the strength of graphene was found to decrease by more than 30% when the number of layers increases from 1 to 8. Here we have investigated such a size-scale effect of GO within the few layer range.

Fig. 4a shows force vs deflection data obtained from the AFM measurements of one monolayer and four multilayer GO membranes (with a similar sag depth of ~ 160 nm) of varying thickness. The force drops in the curves indicate stepwise fracture of the membrane similar to those observed for bilayer GO. Since there is no well accepted AFM deflection analysis for strength determination of multilayers, and the commonly used method is only suitable for monolayers [1], a direct strength measurement here is difficult, especially for our GO samples with deep sag and plastic deformation. Therefore, the fracture force was normalized by the number of layers (F_{fracture}/N) to indicate the general trend in the strength evolution [41]. It was observed that monolayer and bilayer GO maintained similar normalized fracture force. However, scaling up to even 5 layers and further to 12 layers resulted in $\sim 60\%$ deterioration in the normalized fracture force. The number of layers was estimated by averaging at least three SAED measurements on different positions near the center of the membrane. In thicker GO

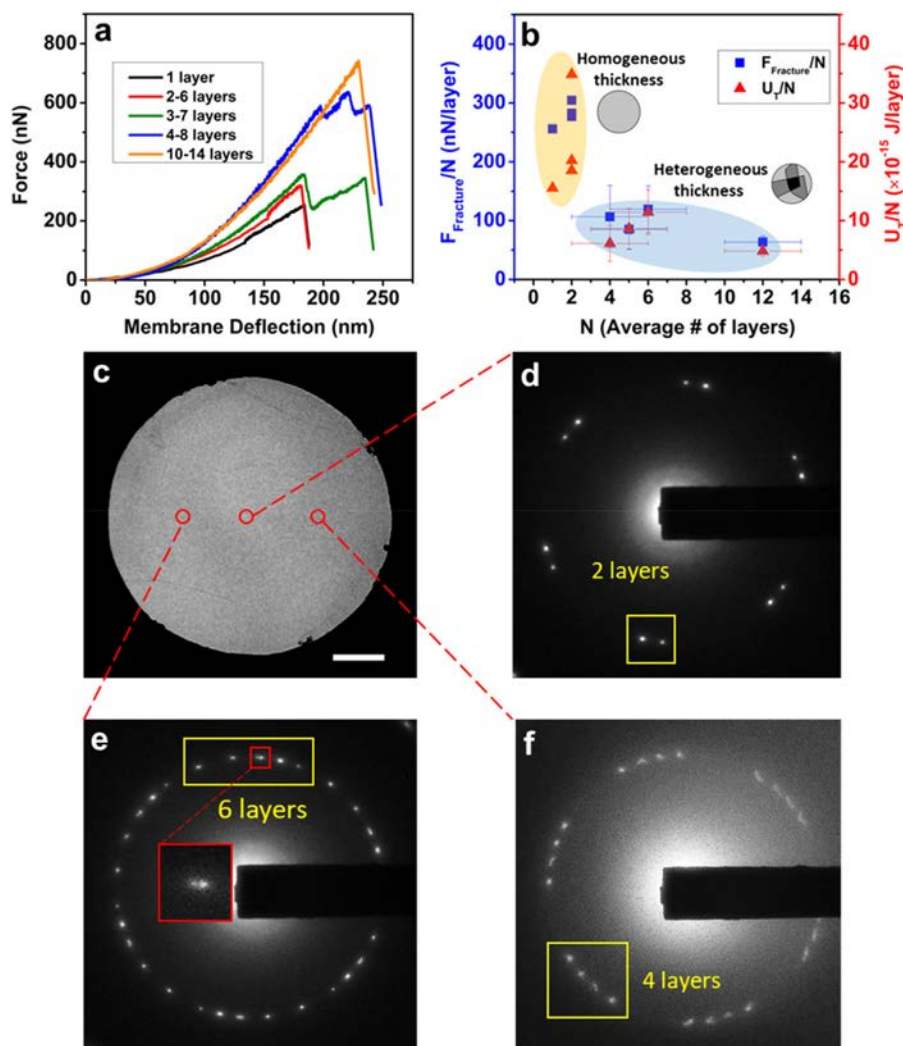


Fig. 4. Multilayer GO fracture. (a) AFM deflection curves of monolayer and multilayer GO. (b) The influence of number of layers on the normalized fracture force and normalized toughness. The normalization is conducted by the number of layers. Horizontal scale bars are the range of number of layers in a membrane, vertical scale bars are the corresponding normalized value calculated based on the horizontal scale bars. (c) Bright field image of a multilayer GO of ~4 layers. Scale bar: 500 nm. (d,e,f) SAED patterns revealing different thickness at different position. (A colour version of this figure can be viewed online.)

multilayers, the likelihood of overlapped diffraction spots are higher, and the existence of more wrinkles, folds, and partial intercalations may influence the diffraction pattern. Therefore, the number of layer estimation may not be as accurate as for monolayer and bilayer counting. However, by averaging multiple measurements, a reasonable estimate of multilayer GO thickness can still be provided. Interestingly, a similar size effect was observed in the friction of 2D materials in which bulk frictional properties were also reached when stacking of more than ~5 layers [42], although this is governed by a different underlying physical mechanism. In addition, the normalized toughness (normalized by the number of layers, U_T/N) exhibits a similar trend with increasing thickness. The strength and toughness deterioration can partly result from finite interlayer sliding energy such that interlayer sliding can occur during the deflection test, similar to multilayer graphene [39,41]. In addition, TEM investigation on ~5 layers GO revealed heterogeneity in thickness across the suspended area, which also contributes to the strength/toughness reduction. In contrast to graphene and boron nitride, GO is often prepared using chemical exfoliation, which does not yield as uniform multilayers as those prepared via mechanical exfoliation. Bright field TEM images in Fig. 4c shows noticeable contrast, revealing different number of layers and

wrinkles in the membrane (see also Supporting Information Figure S5). Further SAED patterns at different positions of the membrane confirmed heterogeneous thicknesses and quantified the varying number of layers (Fig. 4d,e,f).

The effect of local thickness heterogeneity on the mechanics of few layer GO was further investigated using MD simulations. This was achieved by introducing two partially intercalated layers sandwiched between three complete layers (Fig. 5a) in order to study structures with varying local layer thickness similar to those observed experimentally (Fig. 4c–f). Equibiaxial strain-controlled tension results revealed stress/strain concentration near the internal edges of the partial layers (Fig. 5b). The stress-strain curves of the intercalated GO multilayer (Fig. 5c) demonstrated lower strength (or fracture force) as compared with 5 complete layers of GO in both in-plane directions. The stress in Fig. 5c is defined based on the thickness of 5 layers along both in-plane directions. Moreover, due to the partial intercalation, the structure became anisotropic and non-homogeneous, and experienced higher strength (fracture force) along the y direction. To further understand the behavior of each individual layer, the true stress-strain curves of each layer along both in-plane directions are plotted in Fig. 5d and e. Although no direct stretching of layer 2 and layer 4 is applied

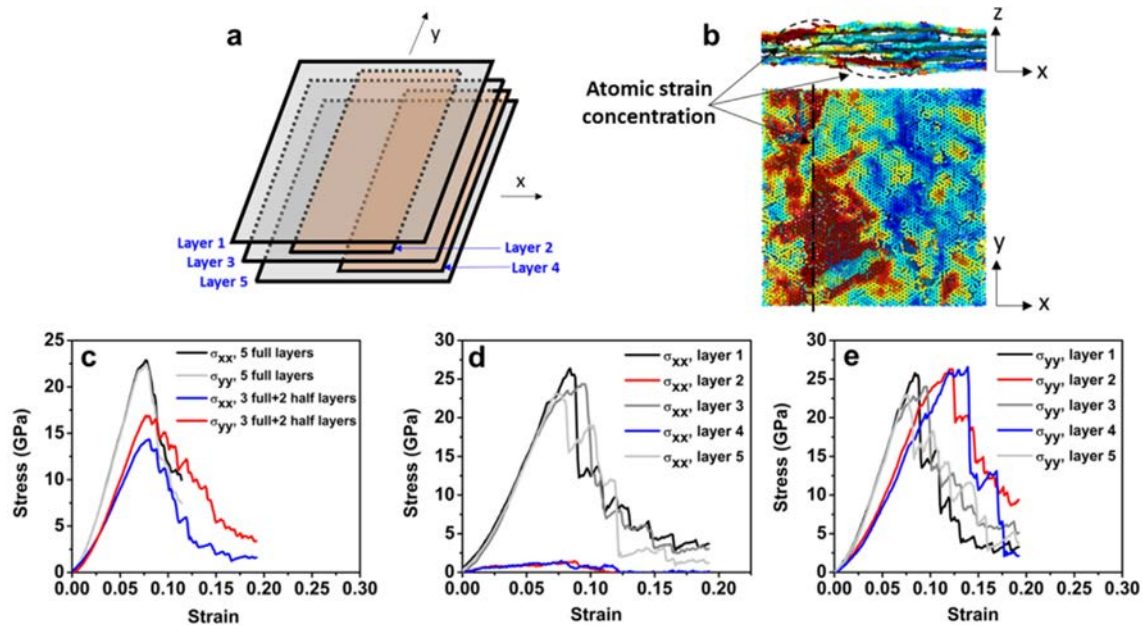


Fig. 5. MD equibiaxial strain-controlled tension of intercalated GO multilayer. (a) Schematic of GO multilayer with 3 full-sized layers (Layer 1, 3, and 5) and 2 half-sized intercalated layers (Layer 2, and 4). Layer 2 aligns at the center of the adjacent layers, and layer 4 aligns at the right of the adjacent layers. (b) Cross-sectional and top view of atomic strain contours showing atomic stress/strain concentration near the edges. (c) Stress-strain curves of the intercalated multilayer GO, as compared with 5 full layers of GO, showing lower strength and anisotropic behavior along in-plane directions. (d,e) True stress-strain curves of each individual layers in the intercalated GO multilayer long x and y direction, respectively. (A colour version of this figure can be viewed online.)

along the x direction, both layers experienced a maximum stress of ~ 1.47 GPa along that direction due to interlayer load transfer and shearing. In the other direction (y axis), layer 2 and layer 4 revealed similar tensile strength as of the complete layers but with higher ductility. The increased ductility was due to the fact that loading in the x direction is much lower than in the y direction so that both intercalated layers were approximately under uniaxial loading rather than equibiaxial loading. Therefore, less compressive strain in the y direction was caused by tension along the x directions due to Poisson's effect.

To further confirm that the loss of strength and toughness observed in experiments were mainly caused by local thickness heterogeneity rather than just stacking more complete layers, direct comparison was made among two complete layers, five complete layers, and partial intercalated five layers. The MD results revealed an average strength of 23.8 GPa and toughness of 1.71×10^{-18} J/nm³ for bilayer GO, which is slightly higher but comparable to that of GO with five complete layers (22.7 GPa for strength and 1.68×10^{-18} J/nm³ for toughness). However, the partially intercalated five layer GO (containing two half-sized layers) exhibits an average strength and toughness of only 15.6 GPa and 1.08×10^{-18} J/nm³, which is $\sim 35\%$ lower than that of the two complete layers. It should also be noted that experimental GO samples can be more complicated in terms of density and distribution of defects, including but not limited to, partial layer intercalation, wrinkles, folds, and point defects. A combination of these defects would likely give rise to more severe anisotropy and heterogeneity, interlayer shearing and stress concentration, thus contributing to more significant reduction of strength and toughness.

4. Conclusions

In summary, the effect of two important structural heterogeneities, i.e., lattice stacking orientation and local thickness variation, on the mechanics of few layer GO was investigated by both

experiments and MD simulations. Highly oxidized bilayer GO with different lattice stacking orientation was prepared and mechanically characterized to fracture. Direct TEM evidence and MD simulations demonstrated decoupled layer cracking and dissimilar cracking pathway of top and bottom layers for misaligned GO. Meanwhile, aligned GO bilayers fractured in a more scattered fashion due to the stochastic distribution of functional groups, but in general, with a larger portion of common cracks shared by both layers, indicating relatively stronger interaction as compared to the misaligned case. However, the results also revealed insignificant effect of lattice alignment on the strength and toughness of GO bilayers, which is ~ 23.5 GPa and $\sim 1.71 \times 10^{-18}$ J/nm³, respectively, for both aligned and misaligned cases. Further scaling up GO to thicknesses of ~ 5 layers and above results in heterogeneities in thickness and $\sim 60\%$ reduction of the normalized fracture force and toughness. MD simulations on partially intercalated and discontinuous GO multilayer revealed anisotropic and heterogeneous stress distribution, as well as stress/strain concentration near the internal edges, which accounts for the strength/toughness loss. In addition to GO, this study can also be practically applied to any other 2D materials and guide mechanical design of layered nano-devices.

Author contributions

§T. Cui and S. Mukherjee contributed equally.

Notes

The authors declare no competing financial interest.

Acknowledgments

The authors acknowledge financial support from the Natural Sciences and Engineering Research Council of Canada (NSERC), the Canada Foundation for Innovation (CFI), the Hart Professorship,

Canada Research Chairs Program, and the Ontario Research Fund: Research Excellence. The authors would also like to acknowledge Rana Sodhi for conducting XPS measurement. XPS and TEM were carried out at Ontario Centre for the Characterisation of Advanced Materials (OCCAM). The MD simulations were carried out using Compute Canada facilities.

Appendix A. Supplementary data

Supplementary data related to this article can be found at <https://doi.org/10.1016/j.carbon.2018.04.074>.

References

- [1] C. Lee, X. Wei, J.W. Kysar, J. Hone, Measurement of the elastic properties and intrinsic strength of monolayer graphene, *Science* 321 (2008) 385–388, <https://doi.org/10.1126/science.1157996>.
- [2] G.-H. Lee, R.C. Cooper, S.J. An, S. Lee, A. van der Zande, N. Petrone, A.G. Hammerberg, C. Lee, B. Crawford, W. Oliver, J.W. Kysar, J. Hone, High-strength chemical-vapor-deposited graphene and grain boundaries, *Science* 340 (2013) 1073–1076, <https://doi.org/10.1126/science.1235126>.
- [3] J.W. Suk, R.D. Piner, J. An, R.S. Ruoff, Mechanical properties of monolayer graphene oxide, *ACS Nano* 4 (2010) 6557–6564, <https://doi.org/10.1021/nn101781v>.
- [4] S. Bertolazzi, J. Brivio, A. Kis, Stretching and breaking of ultrathin MoS₂, *ACS Nano* 5 (2011) 9703–9709, <https://doi.org/10.1021/nn203879f>.
- [5] Y. Yang, X. Li, M. Wen, E. Hacıoğlu, W. Chen, Y. Gong, J. Zhang, B. Li, W. Zhou, P.M. Ajayan, Q. Chen, T. Zhu, J. Lou, Brittle fracture of 2D MoSe₂, *Adv. Mater.* 2 (2016) 1–7, <https://doi.org/10.1002/adma.201604201>.
- [6] J.-W. Jiang, H.S. Park, Negative Poisson's ratio in single-layer black phosphorus, *Nat. Commun.* 5 (2014) 4727, <https://doi.org/10.1038/ncomms5727>.
- [7] D.R. Dreyer, S. Park, C.W. Bielawski, R.S. Ruoff, The chemistry of graphene oxide, *Chem. Soc. Rev.* 39 (2010) 228–240, https://doi.org/10.1007/978-3-319-15500-5_3.
- [8] C. Cao, M. Daly, C.V. Singh, Y. Sun, T. Filleter, High strength measurement of monolayer graphene oxide, *Carbon* 81 (2015) 497–504, <https://doi.org/10.1016/j.carbon.2014.09.082>.
- [9] X. Wei, L. Mao, R.A. Soler-Crespo, J.T. Paci, J. Huang, S.T. Nguyen, H.D. Espinosa, Plasticity and ductility in graphene oxide through a mechanochemically induced damage tolerance mechanism, *Nat. Commun.* 6 (2015) 8029, <https://doi.org/10.1038/ncomms9029>.
- [10] Z. Meng, R.A. Soler-Crespo, W. Xia, W. Gao, L. Ruiz, H.D. Espinosa, S. Keten, A coarse-grained model for the mechanical behavior of graphene oxide, *Carbon* 117 (2017) 476–487, <https://doi.org/10.1016/j.carbon.2017.02.061>.
- [11] W.K. Park, Y. Yoon, Y.H. Song, S.Y. Choi, S. Kim, Y. Do, J. Lee, H. Park, D.H. Yoon, W.S. Yang, High-efficiency exfoliation of large-area mono-layer graphene oxide with controlled dimension, *Sci. Rep.* 7 (2017) 1–9, <https://doi.org/10.1038/s41598-017-16649-y>.
- [12] Y. Xu, W. Hong, H. Bai, C. Li, G. Shi, Strong and ductile poly(vinyl alcohol)/graphene oxide composite films with a layered structure, *Carbon* 47 (2009) 3538–3543, <https://doi.org/10.1016/j.carbon.2009.08.022>.
- [13] K.W. Putz, O.C. Compton, M.J. Palmeri, S.B.T. Nguyen, L.C. Brinson, High-nanofiller-content graphene oxide-polymer nanocomposites via vacuum-assisted self-assembly, *Adv. Funct. Mater.* 20 (2010) 3322–3329, <https://doi.org/10.1002/adfm.201000723>.
- [14] H. Liang, Y. Bu, J. Zhang, Z. Cao, A. Liang, Graphene oxide film as solid lubricant, *ACS Appl. Mater. Interfaces* 5 (2013) 6369–6375, <https://doi.org/10.1021/am401495y>.
- [15] S. Chen, J. Zhu, Q. Han, X. Wang, Graphene Oxide–MnO₂ nanocomposites for supercapacitors, *ACS Nano* 4 (2010) 2822–2830.
- [16] J. Xu, K. Wang, S.-Z. Zu, B.-H. Han, Z. Wei, Hierarchical nanocomposites of polyaniline nanowire arrays on graphene oxide sheets with synergistic effect for energy storage, *ACS Nano* 4 (2010) 5019–5026, <https://doi.org/10.1021/nn1006539>.
- [17] C. Cao, M. Daly, B. Chen, J.Y. Howe, C.V. Singh, T. Filleter, Y. Sun, Strengthening in graphene oxide nanosheets: bridging the gap between interplanar and intraplanar fracture, *Nano Lett.* 15 (2015) 6528–6534, <https://doi.org/10.1021/acs.nanolett.5b02173>.
- [18] D.A. Dikin, S. Stankovich, E.J. Zimney, R.D. Piner, G.H.B. Dommett, G. Evmenenko, S.T. Nguyen, R.S. Ruoff, Preparation and characterization of graphene oxide paper, *Nature* 448 (2007) 457–460, <https://doi.org/10.1038/nature06016>.
- [19] T. Gong, D. Van Lam, R. Liu, S. Won, Y. Hwangbo, S. Kwon, J. Kim, K. Sun, J.H. Kim, S.M. Lee, C. Lee, Thickness dependence of the mechanical properties of free-standing graphene oxide papers, *Adv. Funct. Mater.* 25 (2015) 3756–3763, <https://doi.org/10.1002/adfm.201500998>.
- [20] J. Zhang, J. Xiao, X. Meng, C. Monroe, Y. Huang, J.M. Zuo, Free folding of suspended graphene sheets by random mechanical stimulation, *Phys. Rev. Lett.* 104 (2010) 2–5, <https://doi.org/10.1103/PhysRevLett.104.166805>.
- [21] J.H. Warner, M.H. Rummeli, T. Gemming, B. Buchner, G.A.D. Briggs, Direct imaging of rotational stacking faults in few layer graphene, *Nano Lett.* 9 (2009) 102–106, <https://doi.org/10.1021/nl8025949>.
- [22] S. Latil, V. Meunier, L. Henrard, Massless fermions in multilayer graphitic systems with misoriented layers: Ab initio calculations and experimental fingerprints, *Phys. Rev. B* 76 (2007) 1–4, <https://doi.org/10.1103/PhysRevB.76.201402>.
- [23] M. Dienwiebel, G.S. Verhoeven, N. Pradeep, J.W.M. Frenken, J.A. Heimberg, H.W. Zandbergen, Superlubricity of graphite, *Phys. Rev. Lett.* 92 (2004), <https://doi.org/10.1103/PhysRevLett.92.126101>, 126101–1.
- [24] C. Gómez-Navarro, J.C. Meyer, R.S. Sundaram, A. Chuvilin, S. Kurasch, M. Burghard, K. Kern, U. Kaiser, Atomic structure of reduced graphene oxide, *Nano Lett.* 10 (2010) 1144–1148, <https://doi.org/10.1021/nl9031617>.
- [25] F. Kim, L.J. Cote, J. Huang, Graphene oxide: surface activity and two-dimensional assembly, *Adv. Mater.* 22 (2010) 1954–1958, <https://doi.org/10.1002/adma.200903932>.
- [26] G.J. Silverberg, C.D. Vecitis, Wrinkling and periodic folding of graphene oxide monolayers by Langmuir-Blodgett compression, *Langmuir* 33 (2017) 9880–9888, <https://doi.org/10.1021/acs.langmuir.7b02289>.
- [27] D.C. Marcano, D.V. Kosynkin, J.M. Berlin, A. Sinitskii, Z. Sun, A. Slesarev, L.B. Alemany, W. Lu, J.M. Tour, Improved synthesis of graphene oxide, *ACS Nano* 4 (2010) 4806–4814, <https://doi.org/10.1021/nn1006368>.
- [28] L.J. Cote, F. Kim, J. Huang, Langmuir-blodgett assembly of graphite oxide single layers, *J. Am. Chem. Soc.* 131 (2009) 1043–1049, <https://doi.org/10.1021/ja806262m>.
- [29] J.E. Sader, J.W.M. Chon, P. Mulvaney, Calibration of rectangular atomic force microscope cantilevers, *Rev. Sci. Instrum.* 70 (1999) 3967–3969, <https://doi.org/10.1063/1.1150021>.
- [30] S. Plimpton, Fast parallel algorithms for short-range molecular dynamics, *J. Comput. Phys.* 117 (1995) 1–19, <https://doi.org/10.1006/jcph.1995.1039>.
- [31] A.C.T. Van Duin, S. Dasgupta, F. Lorant, W.A. Goddard, ReaxFF: a reactive force field for hydrocarbons, *J. Phys. Chem. A* 105 (2001) 9396–9409, <https://doi.org/10.1021/jp004368u>.
- [32] N.R. Wilson, P.A. Pandey, R. Beanland, R.J. Young, I.A. Kinloch, L. Gong, Z. Liu, K. Suenaga, J.P. Rourke, S.J. York, J. Sloan, Graphene oxide: structural analysis and application as a highly transparent support for electron microscopy, *ACS Nano* 3 (2009) 2547–2556, <https://doi.org/10.1021/nn900694t>.
- [33] J.C. Meyer, A.K. Geim, M.I. Katsnelson, K.S. Novoselov, D. Obergfell, S. Roth, C. Girit, A. Zettl, On the roughness of single- and bi-layer graphene membranes, *Solid State Commun.* 143 (2007) 101–109, <https://doi.org/10.1016/j.ssc.2007.02.047>.
- [34] L. Gong, R.J. Young, I.A. Kinloch, S.J. Haigh, J.H. Warner, J.A. Hinks, Z. Xu, L. Li, F. Ding, I. Riaz, R. Jalil, K.S. Novoselov, Reversible loss of bernal stacking during the deformation of few-layer graphene in nanocomposites, *ACS Nano* 7 (2013) 7287–7294, <https://doi.org/10.1021/nn402830f>.
- [35] K. Erickson, R. Erni, Z. Lee, N. Alem, W. Gannett, A. Zettl, Determination of the local chemical structure of graphene oxide and reduced graphene oxide, *Adv. Mater.* 22 (2010) 4467–4472, <https://doi.org/10.1002/adma.201000732>.
- [36] D.S. Shin, H.G. Kim, H.S. Ahn, H.Y. Jeong, Y.-J. Kim, D. Odkhuu, N. Tsoqbadrakh, H.-B.-R. Lee, B.H. Kim, Distribution of oxygen functional groups of graphene oxide obtained from low-temperature atomic layer deposition of titanium oxide, *RSC Adv.* 7 (2017) 13979–13984, <https://doi.org/10.1039/C7RA00114B>.
- [37] Q.Y. Lin, Y.H. Zeng, D. Liu, G.Y. Jing, Z.M. Liao, D. Yu, Step-by-step fracture of two-layer stacked graphene membranes, *ACS Nano* 8 (2014) 10246–10251, <https://doi.org/10.1021/nn5033888>.
- [38] C. Cao, S. Mukherjee, J.Y. Howe, D.D. Perovic, Y. Sun, C.V. Singh, T. Filleter, Nonlinear fracture toughness measurement and crack propagation resistance of functionalized graphene multilayers, *Sci. Adv.* 4 (2018), <https://doi.org/10.1126/sciadv.aao7202>.
- [39] X. Wei, Z. Meng, L. Ruiz, W. Xia, C. Lee, J.W. Kysar, J.C. Hone, S. Keten, H.D. Espinosa, Recoverable slippage mechanism in multilayer graphene leads to repeatable energy dissipation, *ACS Nano* 10 (2016) 1820–1828, <https://doi.org/10.1021/acsnano.5b04939>.
- [40] X. Shen, X. Lin, N. Yousefi, J. Jia, J.K. Kim, Wrinkling in graphene sheets and graphene oxide papers, *Carbon* 66 (2014) 84–92, <https://doi.org/10.1016/j.carbon.2013.08.046>.
- [41] A. Falin, Q. Cai, E.J.G. Santos, D. Scullion, D. Qian, R. Zhang, Z. Yang, S. Huang, K. Watanabe, T. Taniguchi, M.R. Barnett, Y. Chen, R.S. Ruoff, L.H. Li, Mechanical properties of atomically thin boron nitride and the role of interlayer interactions, *Nat. Commun.* 8 (2017) 15815, <https://doi.org/10.1038/ncomms15815>.
- [42] C. Lee, Q. Li, W. Kalb, X.-Z. Liu, H. Berger, R.W. Carpick, J. Hone, Frictional characteristics of atomically thin sheets, *Science* 328 (2010) 76–80, <https://doi.org/10.1126/science.1184167>.